Measurement and simulation of deformation and stresses in steel casting

2012 IOP Conf. Ser.: Mater. Sci. Eng. 33 012049

(http://iopscience.iop.org/1757-899X/33/1/012049)

Measurement and simulation of deformation and stresses in steel casting

D Galles[1], C A Monroe[2] and C Beckermann[1]

[1]Department of Mechanical and Industrial Engineering, University of Iowa, Iowa City, IA 52242, USA
[2]Caterpillar Inc., Peoria, IL 61629, USA

E-mail: becker@engineering.uiowa.edu

Abstract. Experiments are conducted to measure displacements and forces during casting of a steel bar in a sand mold. In some experiments the bar is allowed to contract freely, while in others the bar is manually strained using embedded rods connected to a frame. Solidification and cooling of the experimental castings are simulated using a commercial code, and good agreement between measured and predicted temperatures is obtained. The deformations and stresses in the experiments are simulated using an elasto-viscoplastic finite-element model. The high temperature mechanical properties are estimated from data available in the literature. The mush is modeled using porous metal plasticity theory, where the coherency and coalescence solid fraction are taken into account. Good agreement is obtained between measured and predicted displacements and forces. The results shed considerable light on the modeling of stresses in steel casting and help in developing more accurate models for predicting hot tears and casting distortions.

1. Introduction

During cooling of a steel casting, thermal contractions result in dimensional differences between the mold and the final part. A casting is said to contract freely if there are no mechanical interactions between the mold and the contracting steel, in which case the patternmaker's shrink accurately predicts the final dimensions. However, for complex shaped castings, interactions between the mold or cores and the steel generate stresses within the casting, which cause mechanical strains and can result in gross distortions. Additionally, the buildup of stresses at high temperatures may cause hot tears, which are irreversible cracks that form in the semi-solid mushy zone [1]. To minimize these potential problems, accurate stress models that predict the deformations of a steel casting during solidification and cooling can be a valuable tool. Such models require knowledge of the mechanical properties of the steel over the entire range of temperatures and strain rates encountered during casting. The objective of this study is to predict deformations and stresses during steel casting and validate the predictions with data acquired from experiments.

Because the microstructure created during solidification can differ from that in reheated samples, obtaining experimental data in-situ during casting is preferable. However, due to the difficulty of measuring forces and displacements in steel at high temperatures, studies in which stress models of steel casting are validated by in-situ measurements are limited. Monroe and Beckermann [2] acquired force and displacement data during casting of a steel bar to validate a hot tear model. Rowan et al. [3]

used in-situ force measurements in the so-called submerged split chill contraction (SSCC) test to validate a stress model for a solidifying steel shell.

In this study, experiments involving casting of a rectangular steel bar in a sand mold are used to validate the predictions of a stress model. During the experiments, a uni-axial tensile force is applied to the ends of the bar in order to induce mechanical strains. The applied force and the displacements of the ends of the steel bar are measured in-situ as a function of time. In addition to these strained bar experiments, unrestrained bar experiments are performed where no force is applied and the bar is allowed to contract freely. The temperatures in the experiments are predicted using MAGMAsoft [4] and validated through temperature measurements. Stress simulations of the present experiments are performed using the finite-element software ABAQUS [5]. A viscoplastic constitutive model for the mechanical behavior of the steel during solidification and cooling is used that treats the mush as a compressible porous material. The temperature-dependent mechanical properties are estimated from data found in the literature. For the strained bar, the measured forces are included as a boundary condition in the stress model. Measured and predicted end displacements are compared.

2. Description of Experiments

Casting experiments were performed at the University of Northern Iowa's Metal Casting Center. The steel melt was prepared in an induction furnace. The target chemistry was ASTM A216 Grade WCB carbon steel. The molds were made from silica sand bonded with a phenolic urethane no-bake binder. A schematic of the strained bar experiment is shown in figure 1. The dimensions of the cast bar were 12 inches (305 mm) long with a 1 inch (25.4 mm) square cross section. The restrained bar setup is converted to an unrestrained bar setup by removing the restraint, load bolts, restraining bolts, coupling, and turnbuckle.

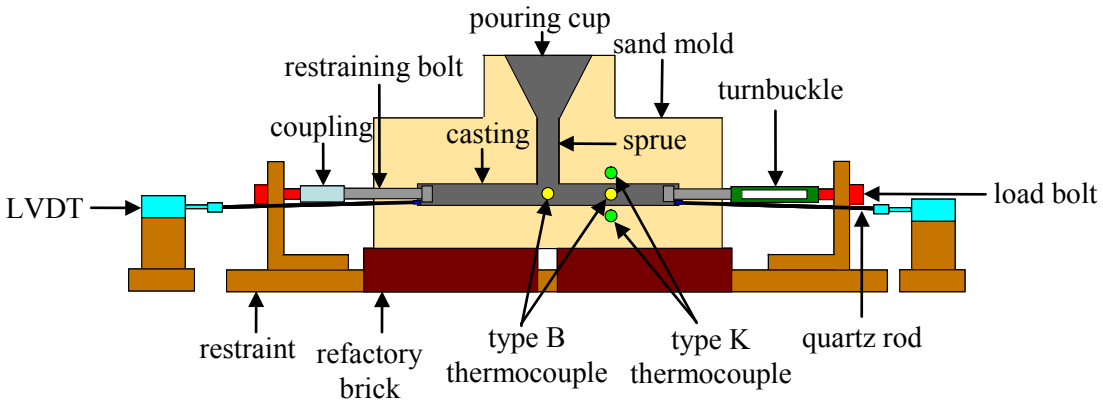

Figure 1. Experimental setup for casting of a strained steel bar.

To acquire temperature, force, and displacement data, a variety of measurement devices were used. Temperatures in the casting and mold were measured using type B and type K thermocouples, respectively. The type B thermocouples were encased in quartz tubing to protect them from the molten steel. The uni-axial force applied to the casting was measured with load bolts located on either side of the mold and anchored by a restraint frame. To transmit the force experienced by the casting to the load bolts, restraining bolts were connected to the load bolt at one end, while the other end extended into the mold cavity. To assure the restraining bolts were firmly embedded in the casting, nuts were threaded onto the ends of the restraining bolts inside the mold cavity. Once poured, the casting was allowed to partially solidify until it reached a level of coherency and could transmit stresses, at which time the turnbuckle was turned to induce stresses in the casting. The forces measured by the two load bolts were in close agreement, indicating that mechanical interactions between the casting and the mold were negligibly small. Axial displacement measurements of the ends of the cast bar were taken with LVDTs located on either side of the mold. In order to avoid damage of

the LVDTs by the heat from the casting, quartz rods were used. Quartz has a very low coefficient of thermal expansion. On each side of the mold, the quartz rod was connected at one end to the LVDT, and the other end was inserted through the mold and extended 3-5 mm into the mold cavity. To ensure the quartz rod did not slip in the casting, the end of the rod inside the mold cavity was bulged into a spherical shape using an oxy-acetylene torch. The length change of the bar was calculated by adding the displacements measured by the two LVDTs.

Overall, three unrestrained and five strained bar experiments were performed. Due to space limitations, plots of all experimental results are not shown here. An example of a measured temperature evolution is shown in figure 2. The measured length changes as a function of time for one unrestrained bar experiment and for one strained bar experiment are shown in figures 4 and 5, respectively. Figure 5 also shows the measured force as a function of time in the strained bar experiment. These plots are discussed in detail below. The thermal results from all experiments were very similar throughout the entire cooling period. The displacement results showed that the evolution of the length change in the three unrestrained bar experiments was very reproducible. The length changes measured in the strained bar experiments varied depending on when and how much stress was induced in the casting by the turnbuckle.

3. Thermal Simulations

Using the experimental casting chemistry, the temperature dependent thermophysical properties and the solid fraction as a function of temperature curve were generated using IDS [6]. These properties include the density, thermal conductivity, and apparent specific heat, which takes into account the latent heat that is released during solidification and solid-state phase changes.

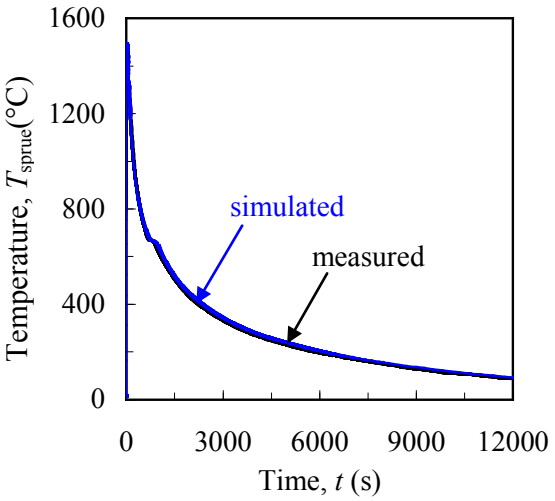

Figure 2. Comparison of measured and predicted temperatures underneath the sprue.

Using these properties along with an estimated pouring temperature and interfacial heat transfer coefficient between the steel and the mold, MAGMAsoft simulations were performed to predict the evolution of the thermal field from the pouring temperature to room temperature throughout the casting. To compare the measured temperatures from the experiments with the predicted temperatures in the MAGMAsoft model, virtual thermocouples were inserted in the model at the locations of the type B thermocouples shown in figure 1. An example of a comparison between measured and simulated temperatures for the thermocouple located below the sprue is shown in figure 2. As the molten steel initially contacts the thermocouple, its temperature increases almost instantaneously from room temperature to approximately 1500 °C. The temperature then rapidly decreases as heat is transferred from the steel to the mold and atmosphere. The temperature continues to decrease until the solid state transformation of austenite to pearlite (at approximately 675 °C). At this point, latent heat is released and the cooling rate of the steel slows to nearly zero for a brief time. This is observed in figure 2 as an inflection point in the curves at approximately 1000 seconds. After the solid state transformation, the temperature again decreases (but at a slower rate) until equilibrium with the room temperature is reached. Through a trial-and-error method, excellent agreement between measured and predicted temperatures was achieved by adjusting the pouring temperature and the interfacial heat transfer coefficient. By adjusting the pouring temperature, the time at which the measured and simulated temperatures reached the solidus temperature was matched exactly. Below the solidus temperature, the measured and predicted temperature curves were matched by decreasing the interfacial heat

transfer coefficient, which was originally set to a constant value of 1000 W/m^{2}K. This decrease is realistic and reflects the formation of an air gap between the casting and the mold during cooling. For the simulated curve in figure 2, the interfacial heat transfer coefficient was decreased at temperatures below 1000 °C.

4. Stress Model

Assuming small strain theory, the total strain, $\boldsymbol{\varepsilon}$, can be decomposed into the elastic (e), thermal (th), and viscoplastic (vp) components as $\boldsymbol{\varepsilon} = \boldsymbol{\varepsilon}_e + \boldsymbol{\varepsilon}_{th} + \boldsymbol{\varepsilon}_{vp}$. Calculations of the elastic and thermal strains were performed using standard procedures and are not discussed here.

The viscoplastic strain is determined from the flow condition. The flow condition limits the maximum stress the steel can hold by keeping the equivalent stress less than or equal to the dynamic yield stress. When the equivalent stress exceeds the dynamic yield stress, the plastic strain is increased to satisfy $\sigma_{eq} = \sigma_{dy}$. In the mushy state, the steel behaves as a compressible material and is modeled using porous media theory, where the equivalent stress is a function of both the von Mises stress and the pressure. Once the steel has completely solidified, it behaves as a regular von Mises material. The equivalent stress is calculated from

$$\sigma_{eq}^2 = A_1\left(g_s^*\right)q^2 + A_2\left(g_s^*\right)p^2 \tag{1}$$

where q is the von Mises stress and p is the pressure. The functions A_1 and A_2 are from the Cocks model and depend on the scaled solid fraction [7, 8], which is given by $g_s^* = g_s^{coal}\left[\left(g_s - g_s^{coh}\right)/\left(g_s^{coal} - g_s^{coh}\right)\right]$, where g_s is the solid fraction, g_s^{coh} is the coherency solid fraction, and g_s^{coal} is the coalescence solid fraction. The coherency solid fraction is the solid fraction at which the material has reached a point of coherency and can transmit stresses. The coalescence solid fraction occurs at a lower temperature and is the solid fraction at which voids begin to coalesce. The values chosen for the coherency and coalescence solid fractions for this study were 0.5 and 0.85, respectively [2, 9]. In the limit where the solid fraction is unity, equation (1) reduces to the von Mises condition, where A_1 is equal to unity and A_2 is equal to zero.

The present viscoplastic constitutive model relates the dynamic yield stress to the viscoplastic strain and strain rate and is given by

$$\sigma_{dy} = \sigma_0\left(1 + \frac{\varepsilon_{eq}}{\varepsilon_0}\right)^n\left(1 + \frac{\dot{\varepsilon}_{eq}}{\dot{\varepsilon}_0}\right)^m \tag{2}$$

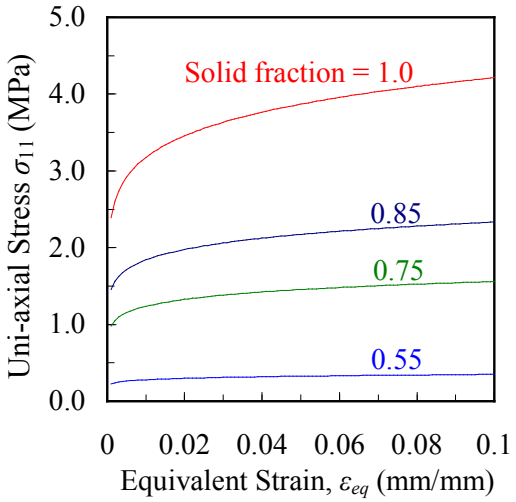

Figure 3. Stress-strain behavior in the mushy state for different solid fractions.

where σ_0 is the initial yield stress, n is the strain hardening exponent, m is the strain rate sensitivity exponent, ε_{eq} is the equivalent plastic strain, and $\dot{\varepsilon}_{eq}$ is the equivalent strain rate. The reference shear strain, ε_0, is calculated from $\varepsilon_0 = \sigma_0 n/E$, in which E is Young's modulus. The reference strain rate, $\dot{\varepsilon}_0$, is given by $\dot{\varepsilon}_0 = A\,exp\left(-Q/RT\right)$ where A is a prefactor, Q is the activation energy, and R is the universal gas constant.

To illustrate the impact of stresses occurring in the mushy state, consider a one-dimensional tensile test. During plastic deformation, $\sigma_{eq} = \sigma_{dy}$ and stress-strain curves can be calculated directly from equations 1 and 2. For uni-axial conditions, the von Mises stress and the pressure can be written in terms of the stress, σ_{11}. Figure 3 shows the uni-axial stress as a function of the equivalent strain at a constant strain rate (10^{-4} 1/s) and

for different solid fraction values. At a solid fraction of 0.55, the mush is very near the coherency limit and therefore can carry only a small load. Increasing the solid fraction from 0.55 to 1.0 significantly increases the load in the mush at a given strain.

5. Mechanical Properties

For the elastic properties, a constant value of 0.3 was used for Poisson's ratio, and the temperature-dependent Young's modulus was taken from Li and Thomas [10].

For the casting experiments in this study, IDS predicted the delta-ferrite to austenite phase transformation to occur at temperatures higher than the coherency solid fraction temperature. Therefore, all viscoplastic deformation in the present experiments occurred in the austenitic phase. The unknown viscoplastic parameters in equation 2 were estimated from experimental stress-strain data for austenitic steel found in the literature. Wray [11] performed tensile tests on reheated plain carbon steel specimens at varying strain rates and carbon contents for temperatures ranging from 850°C to 1200°C. Suzuki et al. [12] performed creep tests on reheated plain carbon steel specimens with a 0.19% carbon content at varying stresses for temperatures ranging from 1200°C to 1400°C. These data were used to estimate the parameters in equation 2. Three parameters (σ_0, n, m) were estimated as linear functions of temperature, while the pre-factor in the reference strain rate, A, is carbon-content dependent [13] and was estimated using a quadratic relationship. The activation energy, Q, was estimated as a temperature-independent constant. All parameters were estimated simultaneously using a Levenberg-Marquardt least-squares minimization between predicted and experimental stresses. The resulting viscoplastic parameters are shown in table 1. They were used from the liquidus temperature down to the solid state transformation temperature of austenite to pearlite (at 675°C). Analysis of the present experimental data revealed that the viscoplastic strain in the strained bars was negligibly small below the solid state transformation temperature. Therefore, to assure no viscoplastic strain was predicted after the solid state transformation, the initial yield stress, σ_0, was set to a very high value at the onset of the solid state transformation.

Table 1. Estimated viscoplastic parameters for austenitic steel, where T is the temperature in °C and $\%C$ is the carbon content.

Parameter	Estimated Value
σ_0	$0.5729 - 1.461\text{x}10^{-5}T$ [MPa]
n	$0.2457 - 6.192\text{x}10^{-5}T$
m	$0.0492 + 9.930\text{x}10^{-5}T$
A	$24870 + 124600(\%C) + 12400(\%C)^2$ [1/s]
Q	353 [kJ/mol]

6. Stress/Displacement Simulations

Stress simulations were performed using ABAQUS, where the viscoplastic constitutive model from section 4 was implemented in a user-defined UMAT subroutine. The temperature fields as a function of time predicted by MAGMAsoft were imported into ABAQUS and mapped onto the finite element mesh. Since mechanical interactions with the mold were negligibly small, stress simulations were performed only for the steel. For the simulation of the strained bar experiments, the measured force was used as a boundary condition. This boundary condition was applied to one end of the bar, while the other end was constrained with a zero-displacement boundary condition.

An example of a comparison between the measured and predicted length changes as a function of time for an unrestrained bar experiment is shown in figure 4. A negative length change represents shrinkage of the bar as it cools. It can be seen from figure 4 that the majority of the shrinkage occurs within the first 400 s after the casting is poured. After 400 s, the solid state transformation from austenite to pearlite begins in the bar and continues until approximately 800 s. During this transformation, the bar expands, which can be seen in figure 4 as a length change increase between

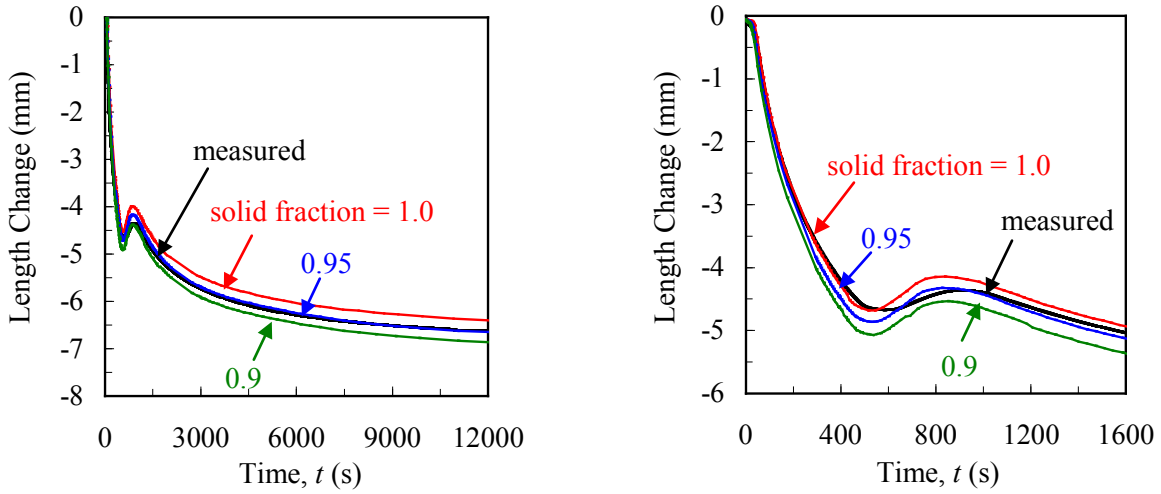

(a) large time scale (b) medium time scale

Figure 4. Comparison of measured and predicted length changes for an unrestrained bar.

400 and 800 s. After the transformation, the bar continues to shrink, albeit at a much slower rate, until it cools to room temperature. At room temperature (i.e., at ~12000 s), the measured length change of the bar is equal to about -6.7 mm, which corresponds to a total shrink of about 2.2%. Because no forces were applied in the unrestrained bar experiments, the length change in the bar is a result of thermal strains only. For the present simulations, the coefficient of thermal expansion was calculated from the density, which in turn was predicted using IDS and is presumed to be accurate. However, the temperature at which integration of the thermal strain is started in the simulations is generally unknown. A lower limit is the solidus temperature (solid fraction of unity), but it could also be higher, such that some liquid is still present in the solid matrix. Therefore, several simulations were performed in which this temperature was varied. The results in figure 4 show that the best agreement between measured and predicted length changes is obtained when integration of the thermal strain is initiated at a temperature corresponding to a solid fraction of 0.95. Finally, the slight disagreement between measured and predicted length changes seen in figure 4(b) during the solid state phase transformation can be attributed to small inaccuracies in the thermal simulation of the experiment.

Figure 5 shows the measured and predicted length changes for one of the strained bar experiments. The measured force, used in the stress simulation as a boundary condition, is also plotted as a function of time. For the first 50 s after the casting is poured, there are no forces applied, and therefore, the bar shrinks like an unrestrained bar during this period. Starting at 50 s, the turnbuckle is turned and the force builds up. As can be seen in figure 5(b), the measured force reaches a value of about 3500 N at the end of the induced straining period (at 123 s). After 123 s, the force continues to build due to thermal contraction of the restrained bar and eventually reaches a value of about 6200 N at 12000 s. This applied tensile force has a significant impact on the length changes of the bar. At about 80 s, the length of the bar begins to increase (at about 80 s). Shortly after the induced straining period, the bar length decreases again. The total measured length change of the strained bar, at 12000 s, is about -4 mm (1.3%). Therefore, the induced straining results in about 2.7 mm of viscoplastic deformation over the length of the bar. For the curve labeled “original simulation”, the viscoplastic parameters listed in table 1 were used. On the large time scale of figure 5(a), the measured and predicted length changes show reasonable agreement, but on the small time scale of figure 5(b), significant differences can be observed during and after the induced straining period. This disagreement can be directly attributed to deficiencies in the calculation of the viscoplastic strain at high temperatures. Through a sensitivity study, it was determined that better agreement between the measured and predicted length changes could be achieved by adjusting the strain rate sensitivity exponent, m, in equation (2), although other

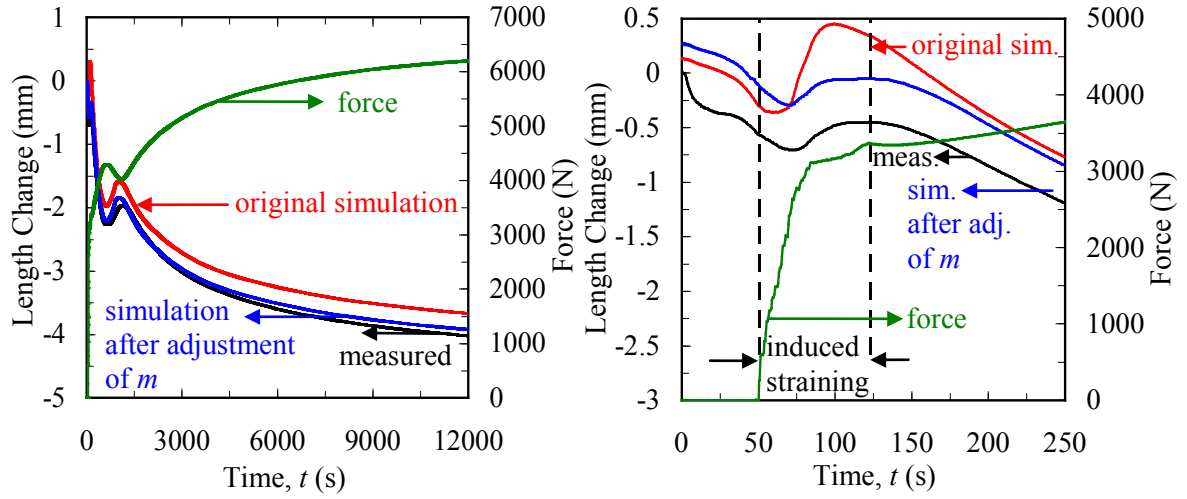

(a) large time scale (b) small time scale

Figure 5. Comparison of measured and predicted length changes for a strained bar.

viscoplastic properties could have been changed too. Figure 6 shows the original and adjusted strain rate sensitivity exponent, m, as a function of temperature. As given in table 1, the original m is a linear function of temperature. The steep decrease between 650°C and 600°C is due to the solid state transformation. The adjusted m is larger than the original m at high temperatures, decreases steeply between 1300°C and 1150°C, and is constant until 650°C. As shown in figure 5, this adjustment of m results in much better agreement between the measured and predicted length changes. The remaining differences are due to slight inaccuracies in the predicted thermal contraction of the bar during the first 50 s. Additional experiments are needed to corroborate the present adjustments in the strain rate sensitivity exponent. However, the comparisons in figure 5 illustrate that even minor changes in the viscoplastic properties can have a large effect on the predicted deformations. Hence, accurate predictions of steel casting distortions can only be made if the viscoplastic properties are known accurately. The deficiencies in the original simulation could also indicate that determining viscoplastic properties from tensile tests of reheated samples, as done in Wray [11] and Suzuki et al. [12], is not appropriate for use in stress models of steel casting. This is because the microstructure and microsegregation in reheated samples is likely to be different from that in just solidified steel.

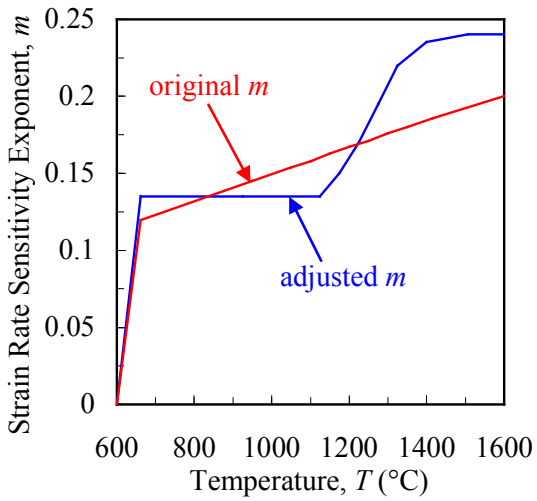

Figure 6. Original and adjusted strain rate sensitivity exponents.

The predicted equivalent plastic strain distribution in the strained bar at room temperature (12000 s) is shown in figure 7. As expected, the majority of the plastic strain occurs in the middle of the bar in the hotspot directly underneath the sprue. This is because the steel was much weaker in the middle of the bar than at the ends when the induced straining commenced. The ends cool more quickly due to the presence of the relatively cold restraining bolts. The large amounts of plastic strain predicted near the ends of the bar are not due to the induced straining but instead are a result of the compressive stresses that build up in the steel as it contracts around the restraining bolt.

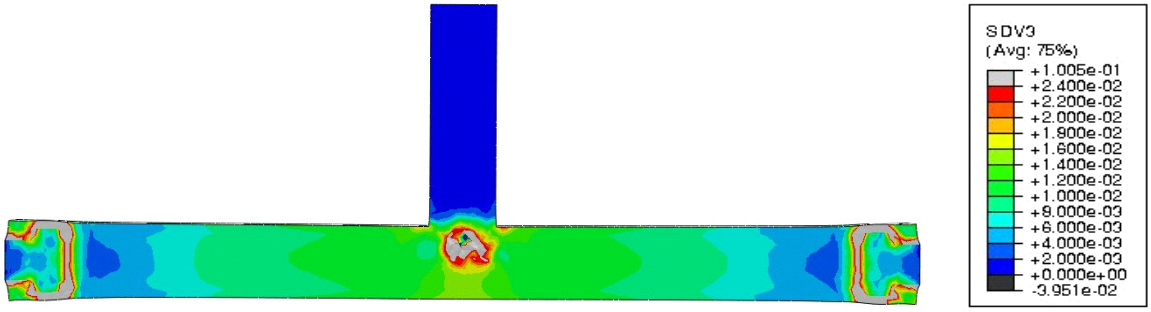

Figure 7. Room temperature equivalent plastic strain in the centre cross-section of the strained bar.

7. Conclusion

The present experiments are well suited to validate stress models of casting. They allow for the in-situ, real time measurement of displacements and forces during solidification and cooling. In addition, stresses of varying amount can be induced in the casting at pre-selected times. The present comparisons between measured and predicted length changes of the steel bar revealed a number of important issues. In particular, the use of viscoplastic properties estimated from stress-strain data for reheated steel samples appears to result in inaccurate deformation predictions. However, a relatively minor adjustment in the strain rate sensitivity exponent led to excellent agreement between measured and predicted length changes under induced straining. The results of this study are encouraging, and significant progress was made in understanding the mechanical behavior of steel during casting and predicting casting distortions and final dimensions.

References

[1] Bichler L, Elsayed A, Lee K and Ravindran C 2008 Influence of mold and pouring temeratures on hot tearing susceptibility of AZ91D magnesium alloy *Int. J. Metalcasting* **2** 45-56
[2] Monroe C and Beckermann C 2005 Development of a hot tear indicator for steel castings *Mat. Sci. and Eng. A* **413-414** 30-6
[3] Rowan M, Thomas B G, Pierer R and Bernhard C 2011 Measuring mechanical behavior of steel during solidification: modeling the SSCC test *Metal. and Mat. Trans. B* **42** 837-51
[4] MAGMAsoft [computer program] Version 4, Kackerstrasse 11, 52072 Aachen, Germany: MAGMA GmbH
[5] Abaqus/Standard [computer program] Version 6.10.2, Providence, RI: Abaqus Inc. ; 2006
[6] IDS [computer program] Version 2.0.0, Espoo, Finland: Helsinki Univ. of Technology; 1999
[7] Marin E B and McDowell D L 2005 A semi-implicit integration scheme for rate-dependent and rate-independent plasticity *Computers and Structures* **63** 30-6
[8] Cocks A C F 1989 Inelastic Deformation of porous materials *J. Mech. Phys. Solids* **37** 693–715
[9] Hardin R A and Beckermann C 2007 Effect of porosity on the stiffness of cast steel *Metal. and Mat. Trans. A* **38** 3041-8
[10] Li C and Thomas B G 2004 Thermomechanical finite-element model of shell behavior in continuous casting of steel *Metal. and Mat. Trans. B* **35B** 1151-72
[11] Wray P J 1982 Effect of carbon content on the plastic flow of plain carbon steels at elevated temperatures *Metal. Trans. A* **13A** 125-34
[12] Suzuki T, Tacke T H, Wunnenberg K and Schwerdtfeger K 1988 Creep properties of steel at continuous casting temperatures *Ironmaking and Steelmaking* **15** 90-100
[13] Wray P J 1980 *Modeling of Casting and Welding Proc.* ed H D Brody and D Apelian (Rindge, NH: The Metallurgical Society of AIME) pp 245-257